ELSEVIER

Nuclear Medicine and Biology 30 (2003) 833–844

NUCLEAR MEDICINE — AND — BIOLOGY

www.elsevier.com/locate/nucmedbio

A review of graphical methods for tracer studies and strategies to reduce bias

Jean Logan*

Chemistry Department, Brookhaven National Laboratory, Upton, NY 11973, USA

Abstract

Graphical techniques provide simple methods for the analysis of data from tracer studies. They provide considerable ease of computation compared to the optimization of individual model parameters in the solution of the differential equations generally used to describe the binding of tracers. The theoretical work of Patlak which was applied to irreversible tracers formed the basis for extensions of graphical techniques to reversibly binding tracers. The advantage of graphical methods is that they are not dependent upon a particular model structure but provide a measure of tracer binding that can be interpreted in terms of a model structure if desired. They provide a visual way to distinguish the type of binding whether reversible or irreversible in the initial studies of new ligands. Conditions under which the graphical techniques can be applied are considered as well as problems encountered with slow binding components. One problem in the use of these methods particularly the method for reversible tracers is the bias generated due to the presence of statistical noise. Some recently proposed techniques for reducing the noise are considered.

1. Introduction

PET and SPET cameras record the time variation of labeled tracer within the body after its introduction generally as a bolus injection. In order to convert this time sequence of radioactivities into one or more numbers that are related to actual physiological processes, it is necessary to apply compartmental models. These models are certainly oversimplifications of the true physiology but nevertheless they allow the estimation of model parameters for the comparison of subjects under different experimental conditions and/or belonging to different groups. In particular, models allow the separation of processes of primary interest such as free receptor concentration from other processes related to tracer uptake. Frequently parameter estimation is done by an iterative nonlinear least squares method requiring a measured plasma input function in which radioactivity of the tracer is measured separately from the metabolites. The differential equations of the compartment models can be linearized and the model parameters can be estimated using standard techniques for linear equations without the requirement of an iterative search (for example the work of Evans and Blomqvist [2,3]). Graphical analysis is a further simplification of general linear methods - it converts the model equations into one equation evaluated at the time points corresponding to the scanning times and provides fewer parameters, namely a slope and intercept. The graphical methods are independent of any particular model structure, although the slope can be interpreted in terms of a combination of model parameters for some model structure. Graphical methods also require an input function although in some instances a reference region can be used in place of plasma input if it is devoid of the specific binding sites. Graphical analysis (GA) methods have been developed for reversibly [4–7] and irreversibly binding tracers [1,8,9]. In the case of irreversible tracers some fraction of the radioactivity is trapped at the binding site for the duration of the experiment. Reversible tracers on the other hand demonstrate uptake and loss from all compartments over the time of the study. The method for irreversible tracers was developed first - the theoretical foundation was provided by Patlak [1,9]. The extension to reversible systems developed by Logan [4] was based on the original work of Patlak. Further refinements have been made by Ichise [7]. The main problem with the use of graphical methods is the bias in the estimated parameters due to noise [10]. Recently some methods for dealing with noise have been proposed [11,12]. We present here a review of the graphical methods, and recent developments in strategies to improve parameter estimation by reducing the bias.

* Tel.: +1-631-344-4391; fax: +1-631-344-7902.
E-mail address: jlogan@bnl.gov (J. Logan).

0969-8051/03/$ – see front matter
doi:10.1016/S0969-8051(03)00114-8

2. Graphical analysis of reversible tracers

In general the compartmental equations can be written using Patlak's notation, [1,9]

$$\frac{d\tilde{C}}{dt} = \tilde{K}\tilde{C} + \tilde{Q}Cp(t) \tag{1}$$

where $\tilde{C}$ is the vector of compartmental concentrations at time t, $\tilde{K}$ is a matrix of the transfer constants between compartments, $\tilde{Q}$ is a vector of plasma to tissue transfer constants which generally consists of one nonzero component designated as K_1. $Cp(t)$ is plasma concentration of unmetabolized tracer (the input function). Using $ROI(t) = \tilde{U}_n^{\tau}\tilde{C} + Vp = \sum_i C_i(t) Vp$ where $ROI(t)$ (region of interest) represents the sum of radioactivities from all compartments and includes the plasma volume fraction, Vp. U_n^{τ} in Patlak's original notation is the tranpose of the vector of 1's that allows the summation of radioactivities. Integrating Eq. (1), multiplying by $\tilde{U}_n^{\tau}K^{-1}$ and rearranging gives

$$\int_0^t ROI(t')dt' = (-\tilde{U}_n^{\tau}\tilde{K}^{-1}\tilde{Q} + Vp\int_0^t Cp(t')dt' + \tilde{U}_n^{\tau}\tilde{K}^{-1}\tilde{C} \tag{2}$$

where $\tilde{U}_n^{\tau}\tilde{K}^{-1}\tilde{Q}$ is the total tissue distribution volume. It is referred to as a volume for historical reason, although it is not actually a volume since an increase in the DV can be due to an increased number of binding sites within the same physical volume. For the 2 tissue compartment model shown below

$$\boxed{Cp(t)} \underset{k_2}{\overset{K_1}{\rightleftarrows}} \boxed{C_1(t)} \underset{k_4}{\overset{k_3}{\rightleftarrows}} \boxed{C_2(t)}$$

both C_1 (nonspecifically bound tracer) and C_2 (specifically bound tracer) occupy the same physical volume, the DV is given by

$$\frac{K_1}{k_2}\left(1 + \frac{k_3}{k_4}\right) \quad \text{(2 tissue components)} \tag{3}$$

where $k_3 \propto Bmax k_{on}$, $Bmax$ is the receptor density and k_{on} is the ligand receptor association constant. The DV for a 1 tissue compartment is given by $K_1/k_2 = \lambda$ where k_2 is the tissue to plasma efflux constant. The ratio $k_3/k_4 = Bmax/Kd$ is also referred to as the binding potential [13]. The Kd from in vivo imaging studies implicitly includes a factor accounting for the fact that only free ligand can bind to the receptor. (It is assumed that there is a very rapid nonspecific component so that k_{on} is given by $fk_{on,}$ where f is the free fraction [13]. There may in addition be a slow nonspecific component.) In the presence of multiple independent binding components, for example different classes of receptors, the DV becomes $\frac{K_1}{k_2}\left(1 + \sum_i \frac{k_1}{K_{-1}}\right)$ where i refers to the type of binding component, k_i is a first order rate constant including the number of available binding sites similar to the definition of k_3 and k_{-i} is the ligand receptor dissociation constant. Thus an increase in the total DV can be due to an increase in the number of tracer binding sites within the same space as seen by the tomograph.

Dividing both sides of (Eq. 2) by $ROI(t)$ gives

$$\frac{\int_0^t ROI(t')dt'}{ROI(t)} = (-\tilde{U}_n^{\tau}\tilde{K}^{-1}\tilde{Q} + Vp)\frac{\int_0^t Cp(t')dt'}{ROI(t)} + \frac{\tilde{U}_n^{\tau}\tilde{K}^{-1}\tilde{C}}{\tilde{U}_n^{\tau}\tilde{C} + Vp} \tag{4}$$

When $\frac{\tilde{C}_n^{\tau}\tilde{K}^{-1}\tilde{C}}{\tilde{U}_n^{\tau}\tilde{C} + Vp}$ becomes constant, a plot of $\frac{\int_0^t ROI(t')dt'}{ROI(t)}$ vs $\frac{\int_0^t Cp(t')dt'}{ROI(t)}$ is linear with a slope given by, $\tilde{U}_n^{\tau}\tilde{K}^{-1}\tilde{Q}$, the total tissue distribution volume. Since the last term in Eq. (4) is not constant due to the time dependence of $\tilde{C}(t)$, the requirement is that it becomes effectively constant after some time t^* so that with further increases in t^* there is no further increase in the slope. The total tissue distribution volume is a measure of the capacity of the tissue to bind the tracer. If the tissue and plasma are in equilibrium, the distribution volume is given by the ratio of the tissue concentration to the plasma concentration $DV = C_{\tau}/Cp$, where $C_{\tau} = \Sigma_i^1 C_i(t)$. Carson et al. [14] have developed methods for achieving a steady state condition by controlling the infusion of tracer after a bolus injection. However if the tracer is given as a bolus injection only, the ratio C_{τ}/Cp is not equivalent to the DV since it is also a function of terms governing the loss of tracer from tissue [4,14]. When the tracer is given as a bolus injection, the DV is given by $\int_0^{\infty} C_{\tau}(t)dt / \int_0^{\infty} Cp(t)dt$ [15]. This not a particularly useful representation since the radioactivities can only be measured at finite times.

The linearity of Eq. (4) is achieved when $\tilde{U}_T^n\tilde{K}^{-1}\tilde{C}/\tilde{U}_n^T\tilde{C}$ approaches a constant value. For the 2 tissue compartment model

$$\frac{\tilde{U}_n^{\tau}\tilde{K}^{-1}\tilde{C}}{\tilde{U}_n^{\tau}\tilde{C}} = -\frac{1}{k_2}\left(1 + \frac{k_3}{k_4}\right) - \frac{C_2(t)}{k_4(C_1(t) + C_2(t)} \tag{5}$$

where

$$\frac{C_2(t)}{(C_1(t) + C_2(t))} \rightarrow \frac{1}{1 + k_4/k_3}$$

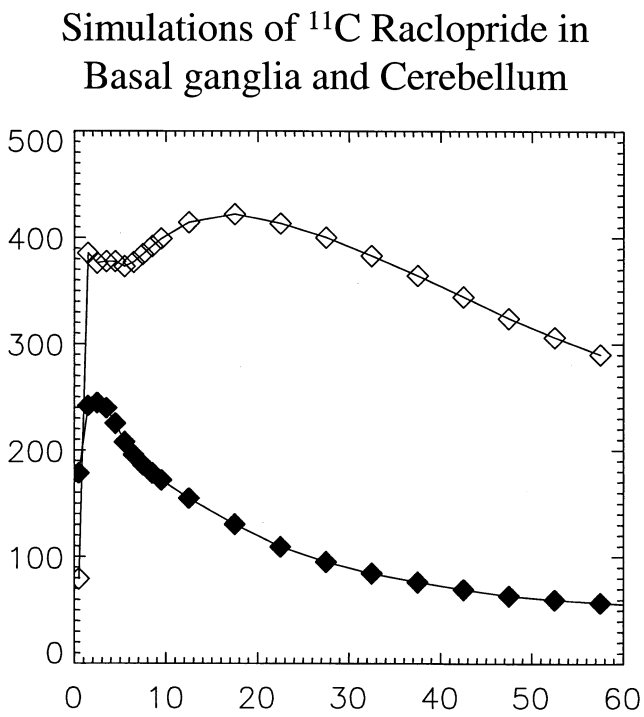

Fig. 1. Typical uptake curves for ^{11}C raclopride in the basal ganglia, a region with D2 receptors, (upper curve) and cerebellum, a frequently used reference region, lower curve. These are simulated data generated from a measured plasma input function using model parameters K_1 = 0.308mL/min/mL, k_2 = 0.776 min$^{-1,}$ k_3 = 0.3171 min^{-1} and k_4 = 0.06 min$^{-1,}$ (DV = 2.49 mL/mL) for the basal ganglia and K_1 = 0.135mL/min/mL, k_2 = 0.34 min$^{-1,}$ k_3 = 0.10 min^{-1} and k_4 = 0.24 min-1, (DV = 0.562 mL/mL) for the cerebellum.

Patlak [1] pointed out that for $t > t'$ a steady state condition is reached for which $\tilde{C} \rightarrow \tilde{K}^{-1}\tilde{Q}Cp(t)$. When this occurs, the intercept becomes $\frac{\tilde{U}_n^{\tau}\tilde{K}^{-2}\tilde{Q}}{-\tilde{U}_n^{\tau}\tilde{K}^{-1}Q}$ which is constant. However, when $\frac{C_2(t)}{(C_1(t)+C_2(t))}$ is changing slowly with time and is close to its asymptotic value, a good estimate of the *DV* can be obtained for times before t', that is for $t > t^*$ where $t^* < t'$. An example is illustrated in Fig. 1 for raclopride, a dopamine (DA) D2 antagonist that binds to the D2 receptors in the basal ganglia. Raclopride is a ligand that has been used extensively in PET research. Simulated data were generated using a measured plasma input function with K_1= 0.308mL/min/mL, k_2 = 0.776 min$^{-1,}$ k_3 = 0.3171 min^{-1} and k_4 = 0.06 min$^{-1,}$ (*DV* = 2.49 mL/mL), for the basal ganglia and K_1 = 0.135mL/min/mL, k_2 = 0.34, k_3 = 0.10 and k_4 = 0.24 min$^{-1,}$ (*DV* = 0.562 mL/mL) for the cerebellum, the reference region. These parameters were taken from a fit to experimental data. For both regions a two tissue compartment model was used. It is frequently necessary to use a two tissue model when fitting the reference region even though there are no specific binding sites. The variation in t^* for these two regions is illustrated in Fig 2. For the basal ganglia t^* is on the order of 25 min and for the cerebellum t^* is 15 min. In general t^* depends upon k_4 (and/or k_2) which determines how fast the ratio $C_2/(C_1+C_2)$ reaches its asymptotic value (Eq. (5)). It also determines the required scanning length. The variation in the time dependence of the ratio $C_2/(C_1+C_2)$ as a function of k_4 is

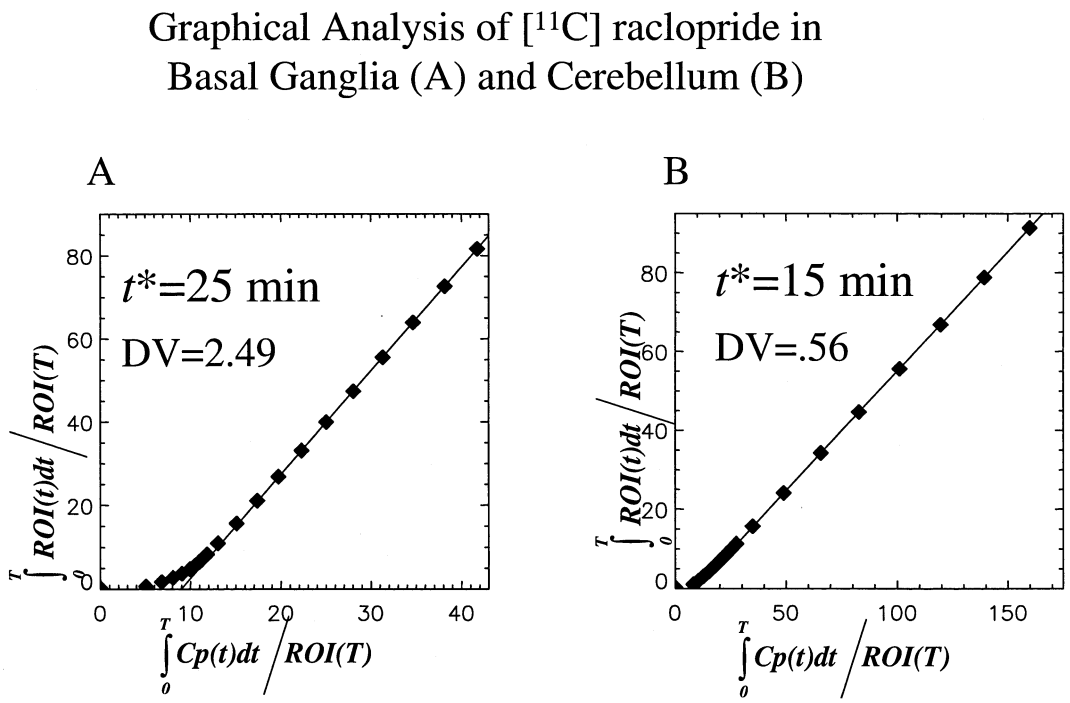

Fig. 2. Graphical analysis of the data from Fig 1. Time constant for start of the linear analysis for basal ganglia is 25 min and for cerebellum is 15 min. The shorter time for the cerebellum is due to its more rapid kinetics as illustrated in Fig 1.

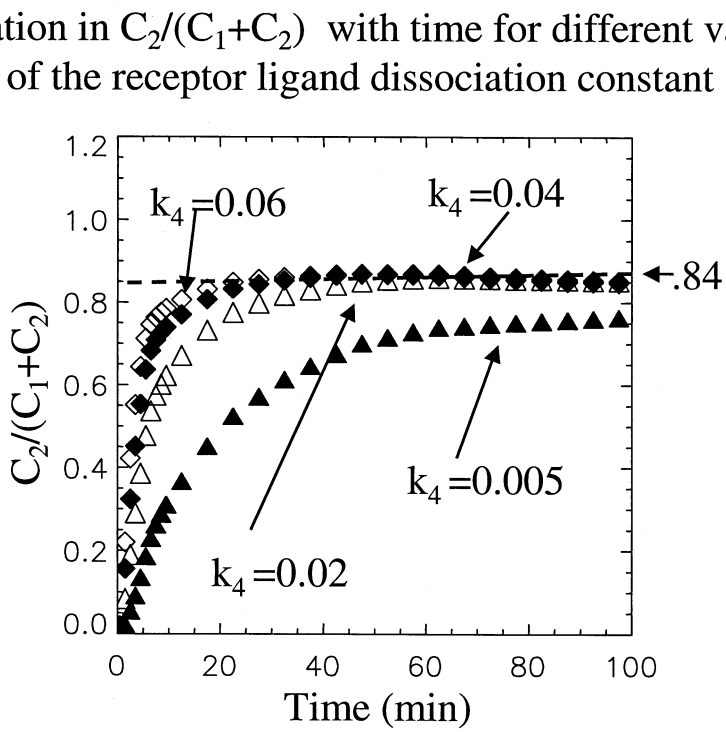

Fig. 3. Variation in the time dependence of the "intercept" of Eq. (4) with different values of k_4, the receptor-ligand dissociation constant. Model parameters used in the simulations were K_1= 0.308mL/min/mL, k_2 = 0.776 min^{-1}, the k_4 values used were 0.06, 0.04, 0.02, 0.005 min^{-1} (k_3 was also varied to maintain the same DV, 2.49 mL/mL). The asymptotic value for $C_2/(C_1+C_2)$ was 0.84.

illustrated in Fig 3 for k_4 values of 0.06, 0.04, 0.02, 0.005 min^{-1} (keeping constant k_3/k_4 and the *DV*). The asymptotic value of $C_2/(C_1 + C_2)$is 0.84. For k_4 = 0.06, and 0.04 min^{-1}, t^* is on the order of 25 min. For k_4 = 0.02 min^{-1} the time required is longer ~ 35 to 40 min. To determine t^*, progressively longer initial times are used until the *DV* doesn't change. Clearly with a very slow k_4, for example k_4 = 0.005 min^{-1} in Fig 3, the ratio $C_2/(C_1 + C_2)$ has not reached the asymptotic value. When $C_2/(C_1 + C_2)$ is less than the asymptotic value, the *DV* is underestimated, since the absolute value of the "intercept" is less than the true value. The graphical analysis for this example is illustrated in Fig 4 with k_4=0.005. Taking an early slope with t^* = 80 min and a final time of 120min the *DV* is 2.01mL/mL an underestimate of 20%. Using all the simulated data points from 80 to 255 min the *DV* is only underestimated by 9%, (*DV* = 2.26). With t^* = 220 min a value close to the correct value is obtained, 2.42mL/mL. The simulations were carried out to 255 min. Two points emerge from this example. Even if t^* is less than the time at which the effective steady state is reached, if a sufficient number of points are included in the calculation after the this time, the error in the estimate of the DV is less. Secondly it will be difficult to obtain true estimates of the *DV* for ligands with slow kinetics that are labeled with short half-life tracers such as C11. In this example if the total scanning time were only 1.5 hours, the *DV* would be significantly underestimated.

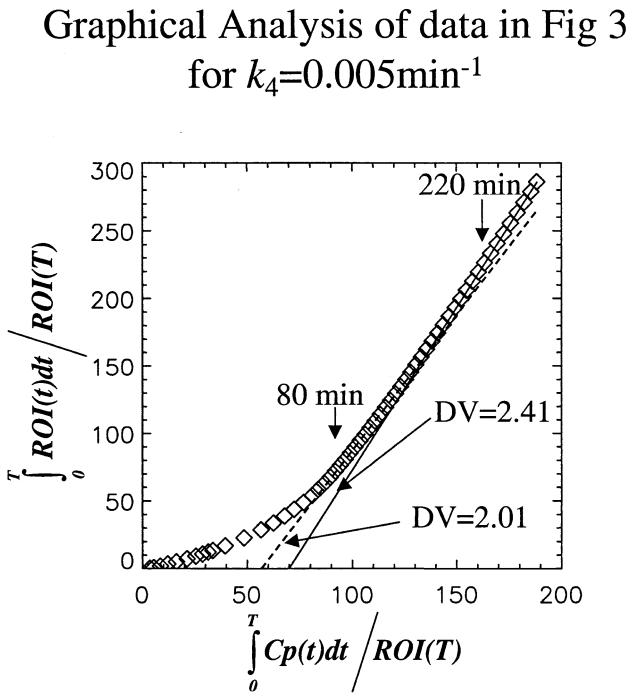

Fig. 4. Graphical analysis of simulated data in Fig 3 with K_1 = 0.308mL/min/mL, k_2 = 0.776, k_3 = 0.0264 and k_4 = 0.005 min^{-1}, *DV* = 2.49 mL/mL. Using t* = 80 min with end time 120 min the *DV* is underestimated by 20%. With t* = 220min and end time 255 min, the *DV* is 2.41mL/mL, close to the true value.

When this occurs the *DV* can appear to be a function of blood flow as in the example discussed below.

In summary the operational equation for the GA of reversible tracers using a plasma input is given by

$$\frac{\int_0^t ROI(t')dt'}{ROI(t)} = DV\frac{\int_0^t Cp(t')dt'}{ROI(t)} + int \qquad (6a)$$

where linearity is achieved for t^* when the intercept (*int*) is effectively constant. An alternative form of the GA equation is obtained from Eq. (4) by dividing by $Cp(t)$ instead of the *ROI* value giving

$$\frac{\int_0^t ROI(t')dt'}{Cp(t)} = DV\frac{\int_0^t Cp(t')dt'}{Cp(t)} + int_b \qquad (6b)$$

The problem with this formulation as discussed above is that the true steady state condition must apply before linearity is achieved and this generally requires somewhat longer times than when *ROI* is used in the denominator.

3. Distribution volume ratio

Generally the *DV* ratio (*DVR*) or binding potential, which can be derived from the *DVR* are used for comparing data sets. The *DVR* is the ratio of the *DV* in a receptor region to that of a reference region. This generally provides better reproducibility on test/retest than comparing either the *DV* or the receptor parameter k_3. If the *DV* of the reference region has one tissue compartment, then the binding potential (*BP*) can be derived from the *DVR*

$$DVR = \frac{\lambda^{ROI}}{\lambda^{REF}}(1 + BP)$$

where $\lambda = K_1/k_2$ for *ROI* or *REF*, if this ratio is the same in both tissues, which is a common assumption, then *BP=DVR-1*. However, in many cases the reference region is not well described by a single tissue compartment so that the *DVR* contains in addition to the rapid nonspecific binding extra terms corresponding to a slower nonspecific binding component with equilibrium constant (*NS*),

$$DVR = \frac{\lambda^{ROI}(1 + NS + BP)}{\lambda^{REF}(1 + NS^{REF})}.$$

If λ and *NS* are the same in both tissues, $DVR = 1 + f^{NS} BP$ where $f^{NS} = 1/(1 + NS)$. The interpretation of the *BP* derived from the *DVR* is somewhat different in this case since it is modified by the factor f^{NS}.

4. Graphical analysis using a reference region

We can extend graphical analysis to obtain *DV* ratios directly without blood sampling by using a reference region in place of the plasma integral. This can be done by rearranging the graphical analysis equation for the reference region to solve for the plasma integral in terms of the reference region radioactivity. Rearranging Eq. (6a) where *REF* is used in place of *ROI* gives

$$\int_0^t Cp(t')dt = \frac{1}{DV^{REF}} \left[\int_0^t REF(t')dt - int^{REF} REF(t)\right]. \qquad (7a)$$

Substituting for the integral of the plasma in the equation for the receptor *ROI* Eq. (6a) gives

$$\frac{\int_0^t ROI(t')dt'}{ROI(t)} = \frac{DV}{DV^{REF}} \cdot \left[\frac{\int_0^t REF(t')dt' — int^{REF} REF(t)}{ROI(t)}\right] + int^{ROI}. \qquad (7b)$$

If the reference region is a one tissue compartment model, then DV^{REF} is given by K_1/k_2 and int^{REF} is $-1/k_2$. This, however, is not a requirement for the method. For simplicity of expression let $int^{REF} = 1 - 1/k_2'^{REF}$, which in the case of a two tissue compartment model is given by Eq. (5) so that

$$\frac{1}{k_2'^{REF}} = \frac{1}{k_2^{REF}}\left(1 + \frac{k_3^{REF}}{k_4^{REF}}\right) + \frac{1}{k_4^{REF}(1 + k_4^{REF}/k_3^{REF})}.$$

Replacing $k_2'^{REF}$ with an average over subjects, $\bar{k}_2'^{REF}$, then

$$\frac{\int_0^t ROI(t')dt'}{ROI(t)} = DVR\left[\frac{\int_0^t REF(t')dt' + REF(t)/\bar{k}_2'^{tREF}}{ROI(t)}\right] + int^{ROI} + \delta$$

where the error term is $\delta = DVR\left(\frac{1}{k_2^{REF}} - \frac{1}{\bar{k}_2'^{REF}}\right)\frac{REF(t)}{ROI(t)}$. The operational equation is

$$\frac{\int_0^t ROI(t')dt'}{ROI(t)} = DVR \cdot \left[\frac{\int_0^t REF(t')dt' + REF(t)/\bar{k}_2'^{REF}}{ROI(t)}\right] + int' \qquad (8)$$

In many cases the term $REF(t)/\bar{k}_2'^{REF}$ may be omitted. Fig 5

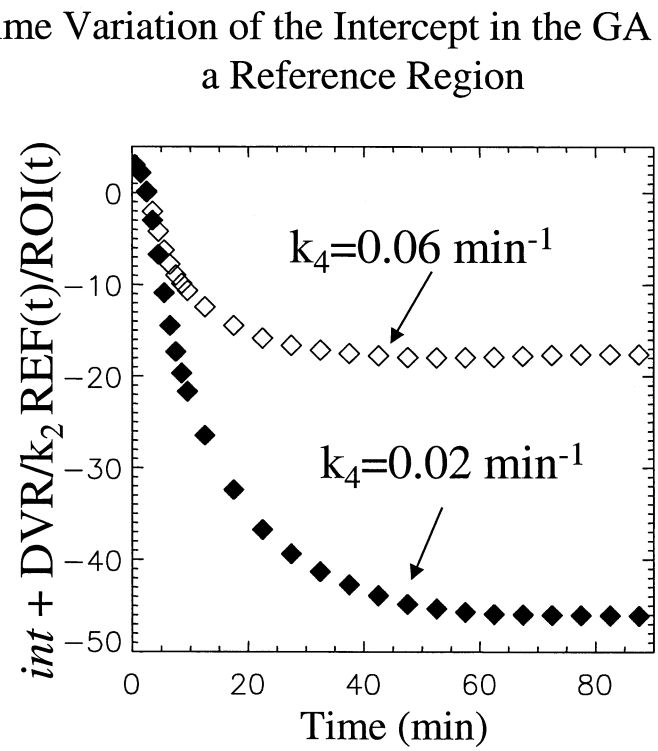

Fig. 5. The time variation of the "intercept" of the GA using a reference region for the raclopride example of Fig 3 with $k_4 = 0.06$ and $0.02 min^{-1.}$ A somewhat longer time is required for the slower dissociation (lower curve) to become constant.

illustrates the time variation of the intercept for the raclopride example given above with $k_4 = 0.06$ and $0.02\ min^{-1.}$

An alternative form of this equation has been proposed by Ichise and Ballinger [6], a bilinear analysis where b and b' correspond to int^{ROI} and $-(DVR\ int^{REF)}$ respectively in Eq. (7b)

$$\frac{\int_0^t ROI(t')dt'}{ROI(t)} = DVR\left[\frac{\int_0^t REF(t')dt'}{ROI(t)}\right] + b'\frac{REF(t)}{ROI(t)} + b \qquad (8b)$$

b and b' become constant for $t > t^*$.

5. Graphical analysis of irreversible tracers

Some tracers bind irreversibly, for example the monoamine oxidase (MAO) tracers [^{11}C] L-deprenyl, and the deuterium substituted [^{11}C] L-deprenyl-D2 [16–18] are suicide inhibitors for MAO B and similarly [^{11}C] clorgyline and [^{11}C]clorgyline-D2 irreversibly inhibit MAO A [19]. Other tracers may appear irreversible over the course of the PET experiment because the ligand receptor dissociation is very slow. In addition to Eq. (1) which describes the reversible parts of the system, the accumulation into the irreversible compartment is given by the general equation (1)

$$\frac{dTr}{dt} = \tilde{U}_n^{\tau}\tilde{G}\tilde{C}$$

where $\tilde{G}$ is a matrix of transfer constants from the reversible compartments to the irreversible compartment and Tr is the concentration in the trapped compartment. The operational equation for the graphical analysis of irreversible tracers is

$$\frac{ROI(t)}{Cp(t)} = Ki\frac{\int_0^t Cp(t')dt'}{Cp(t)} + fVe + Vp \qquad (9)$$

where Ki is the influx constant describing the transfer of tracer from the plasma compartment to the irreversible compartment. The term fVe corresponds to $\tilde{U}_n^T(\tilde{G}\tilde{K}^{-1}+I)\tilde{C}/Cp(t)$. The "intercept" contains the fraction f of the tracer in the reversible compartments that goes back into the plasma and leaves the system [1]. Here $ROI(t) = \sum_i C_i(t) + Tr.$ and Ve is given by $\sum_i C_i(t)/Cp(t)$ which for some time $t > t'$ becomes constant, that is, the steady state condition for the reversible components must apply. In the steady state condition $f(t)$ also becomes constant. If the binding is not strictly irreversible, that is if there is a slow loss from the irreversible compartment, then Eq. (9) can be modified to take this into account [9]. Using k_b as a rate constant for the loss from the irreversible compartment and assuming $k_b << Ki$ the graphical analysis becomes

$$\frac{ROI(t)}{Cp(t)} = Ki\frac{\int_0^{\tau} e^{-k_b(t'-t)}Cp(t')dt'}{Cp(t)} + fVe + Vp.$$

In order to estimate the value of $k_{b,}$ the data should first be plotted according to Eq. (9). If it does not have a linear portion but appears concave, then $k_b > 0$. By increasing k_b in small increments and plotting, a value can be found for which the graphical analysis is linear for some time $t > t'$.

Patlak and Blasberg, [9] developed a graphical analysis for irreversible systems using a reference region. This can also be derived using Eq. (7a) for the plasma integral and substituting into Eq (9) and dividing by *REF*(*t*),

$$\frac{ROI(t)}{REF(t)} = \frac{Ki}{(DV^{REF})}\frac{\int_0^{t} REF(t')dt'}{REF(t)} - \frac{int^{REF}Ki}{DV^{REF}} + \frac{Cp(t)}{REF(t)}(fVe + Vp)$$

The slope is given by Ki/DV^{REF}. Since *Ve* is defined as, $\sum_i^1 C_i(t)/Cp$ where the sum is over the reversible components in the region containing the trapped ligand, the last term becomes $f\frac{\sum_i C_i(t)}{REF(t)}$, neglecting *Vp*. When these terms become constant, the graphical analysis equation applies. As with the reversible system this will be true for the steady state case.

6. Some problems with irreversible tracers

A two tissue compartment model with one compartment representing the trapped component as illustrated below

$$\boxed{Cp(t)} \underset{k_2}{\overset{K_1}{\rightleftarrows}} \boxed{C_1(t)} \xrightarrow{k_3} \boxed{C_2(t)}$$

has $Ki = \frac{K_i k_3}{k_2 + k_3} = \frac{K_1 \lambda k_3}{K_1 + \lambda k_3}$. The ratio $K_1/k_2 = \lambda$ is not a function of blood flow [20], however, *Ki* depends upon blood flow since K_1 is a function of blood flow and capillary permeability [21]. An increase in *Ki* could be due to either an increase in blood flow or an increase in tracer binding. Since it is usually the change in tracer binding that is of primary interest it is necessary to separate these two processes. This means that *Ki* by itself is not sufficient to characterize the ligand binding, K_1 needs to be determined also. If K_1 is known, then $\lambda k_3 = \frac{K_1 K_i}{K_1 - Ki}$. Obviously K_1 must be greater than *Ki*. If $\lambda k_3 \gg K_1$. then *Ki* is primarily dependent upon K_1 and conveys little information about λk_3 (enzyme/receptor concentration). This is referred to as flow-limited and is a characteristic of the tracer not the method of analysis.

7. Problems with linear methods

7.1. Using a plasma input function

The differential equations used to describe movement of tracer between plasma and tissue compartments can be linearized so that the model parameters are more easily determined by solving a set of linear equations [2,3]. For example the differential equation for one tissue compartment model

$$\frac{dC_1(t)}{dt} = K_1 Cp(t) - k_2 C_1$$

becomes

$$C(t_i) = K_1\int_0^{t_i} Cp(t)dt + k_2\int_0^{t_i} C_1(t)dt + \xi_i$$

where ξ_i are the error terms. Since the error terms are not statistically independent, the parameter estimates may be biased [22,23]. Feng [22] proposed a method for eliminating the bias but this applies to a particular model structure. Similarly the GA equation Eq. (6a) has been shown to give a biased estimates of the *DV* [10,11]. In traditional least squares estimation the independent variables are assumed to be noise-free. Correlated noise appears in both the independent and dependent variables. Furthermore, as pointed out by Ichise [11] the GA method for reversible tracers Eq. (6a) contains the noisy tissue radioactivity as a denominator in the independent variable, leading to a biased estimate. Logan [12] proposed a method for reducing the bias by smoothing the data using the Feng 1 tissue compartment model in two parts and then applying graphical analysis. This however is a more complicated calculation. Recently two ideas have been proposed to reduce this bias while maintaining the simplicity of the calculation. One is the total or perpendicular least squares (LS) that minimizes the perpendicular distance squared between the point and the fitted line [24]. This method takes into account the noise in the independent as well as dependent variables. Ichise points out that the perpendicular LS method is the same as the total LS method of Van Huffel and Vandewalle [25]. The method proposed by Ichise [11] rearranges the GA equation into a multilinear regression form (Eq. (10) so that the independent variable is the integral of *ROI* which is subject to less variability than the *ROI* value,

Table 1
Comparison of three formulations of the GA method

Noise	Model	t CV	% Bias
.04	MLS	.041	0
	TLS	.04	−1.3
	GA	.039	−1.7
.12	MLS*	.17	4
	TLS	.11	−7
	GA	.09	−10
.28	MLS*	.26	4.3
	TLS	.14	−20
	GA	.12	−23

The coefficient of variation (CV) and %bias (estimated value - true value/true value × 100) are given for three different formulations of the graphical analysis method for reversible ligands.

* Indicates that values <0 and >5 were eliminated for noise level .28 (420/500).

$$ROI(T) = \frac{DV}{b}\int_0^t Cp(t')dt' + \frac{1}{b}\int_0^t ROI(t')dt' \qquad (10)$$

A third method was proposed by Ichise [11], but this is based on a particular model and is not considered here although it seems to be more generally applicable. Using the previous raclopride example with $DV = 2.49$, $K_1 = 0.308$ mL/min/mL, $k_2 = 0.776$, $k_3 = 0.317$ and $k_4 = 0.06$ (min^{-1}), the 3 linear methods, GA, GA with perpendicular distance formulation (TLS) and the multilinear form of Eq. (10) (MLS) are compared in Table 1. Introducing gaussian noise (mean of zero and standard deviation of one), that takes into account the scan duration (Δt_i) and isotope decay (B) with level of noise controlled by the scale factor *Sc*,

$$Sc\left(\frac{e^{\beta t_i}ROI(t_i)}{\Delta t_i}\right)^{1/2}$$

500 data sets were generated for each different value of *Sc*. Fig. 6 shows the results for the three methods in terms of the average and standard deviation. The results are given as a function of noise $\langle f_N^{ROI}\rangle_{N,t_i}$, where

$$(f_N^{ROI})_{N,t_i} = \left\{\frac{|\Delta ROI(t)|}{ROI_\tau(t)}\right\}$$

is the average of the absolute value of the difference between the noisy value and the true value, $|\Delta ROI(t)|$ divided by the true value, $ROI_T(t)$. Both forms of the GA underestimate the *DV* with increasing noise, the TLS method is only slightly better than the GA method. The MLS tends to a slight overestimate with noise but with increasing variability. For the MLS method, estimates outside of reasonable values were excluded (values <0 and >5). At low noise levels all methods are about the same in terms of the coefficient of variation, CV, (SD/mean) and the bias (estimated value – true value). At intermediate noise levels GA is 10% below the true value with 10% CV while the MLS gives an unbiased estimate of the mean but with a higher CV, 17%. At high noise the CV for MLS is 26% and the bias for GA is also on that

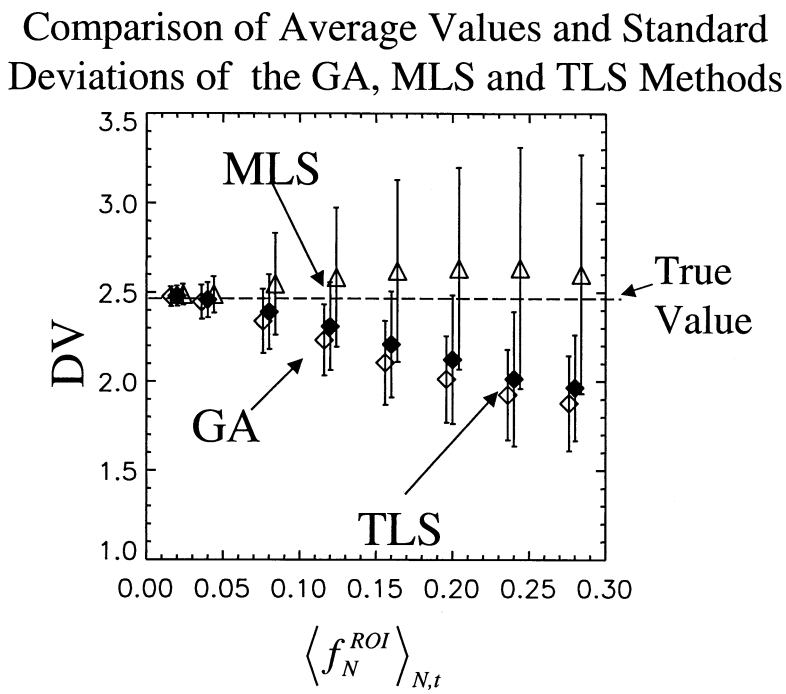

Fig. 6. A comparison of the average value and standard deviation of the MLS, TLS and GA methods. The true value is indicated by the dashed line. The GA method underestimates the DV with increasing noise. The TLS method is only slightly better. The MLS method has less bias with increasing noise but the variability in terms of the standard deviation is increased over that of the GA and TLS.

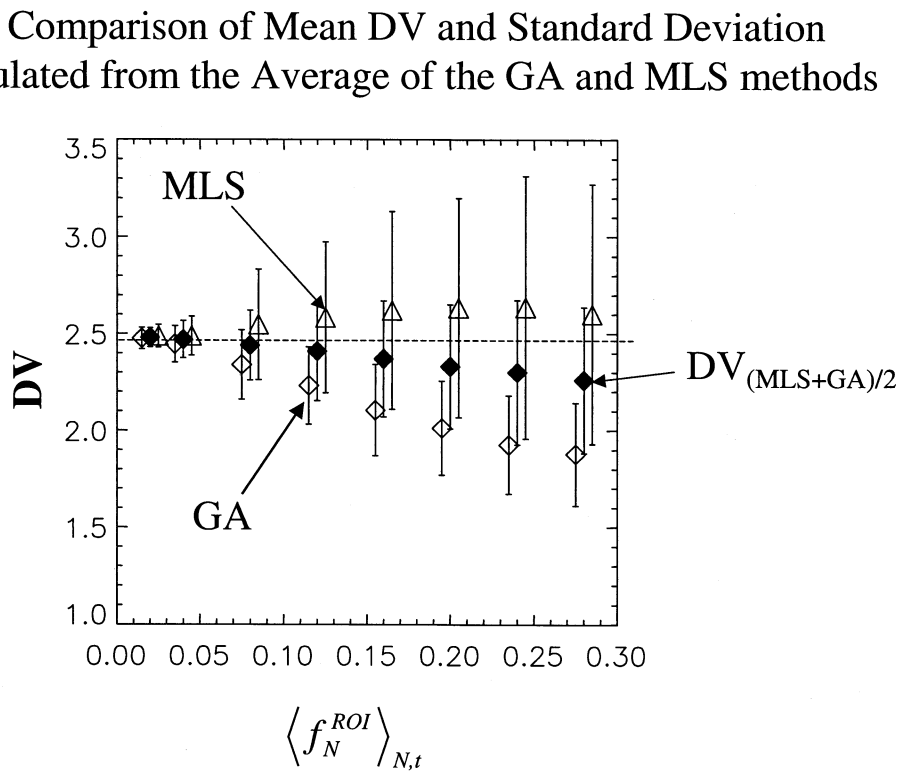

Fig. 7. Results from the average of the GA and MLS methods. The standard deviation is less than with the MLS and the bias is less than the GA. The true value is indicated by the dashed line, the average is indicated by $DV_{(MLS+GA)/2.}$

order, 23%. In order to improve the CV and reduce the bias in the GA method, an average of the DV for both methods was compared (Fig 7). This appears to extend the noise range over which the bias and CV are reasonably small. For example the bias is −5% at noise level 0.16 with CV 13% for the average of MLS and GA compared to a bias of –15% and CV 11% for GA at the same noise level.

Results for the GA method using the plasma tracer levels in the denominator, Eq. (6b) are given in Table 2. The initial time t^* was increased from 25 min as was used for the original method Eq. (6a) to 35 min. This gave 5 points for the determination of the slope. The *DV* is slightly underestimated with 2.46 instead of 2.49 for data without added noise. Using times from 30 min the slope was 2.40 mL/mL. Interestingly there is little variation in the average value over all noise levels and the CV is comparable to the GA method Eq. (6a). The problem is that for many ligands it may not be possible to find t^* such that there are a sufficient number of points for which the intercept is changing slowly enough to allow a reasonable DV estimate. Raclopride happens to be a particularly good tracer in this sense.

Table 2
GA method for RAC example using Eq. (6b)

Noise	DV	STD	CV
0.00	2.46		
0.04	2.46	0.046	0.019
0.08	2.46	0.092	0.037
0.12	2.46	0.136	0.055
0.16	2.45	0.180	0.074
0.20	2.45	0.130	0.094
0.24	2.43	0.287	0.117
0.28	2.43	0.330	0.137

Average DV, standard deviation (STD) and coefficient of variation (CV) for GA method of Eq. (6b) using plasma value instead of ROI in the denominator.

These model independent methods are potentially useful for generating pixelwise images due to the speed of calculation as well as the model independence. In order to reduce the bias and variability, an average of values determined from some subset of these different methods may be superior to any one of them. Also other methods that combine similar pixels to reduce noise may be useful. Recently we used a method in the generation of images of the MAO tracer clorgyline combining pixels within a local region if they were within a certain fraction of the time integrated image (Logan et al, 2002). The idea is that pixels that are within close proximity and also within a certain range of the time integrated image are functionally related. Other techniques for grouping pixels have been used to reduce noise [26].

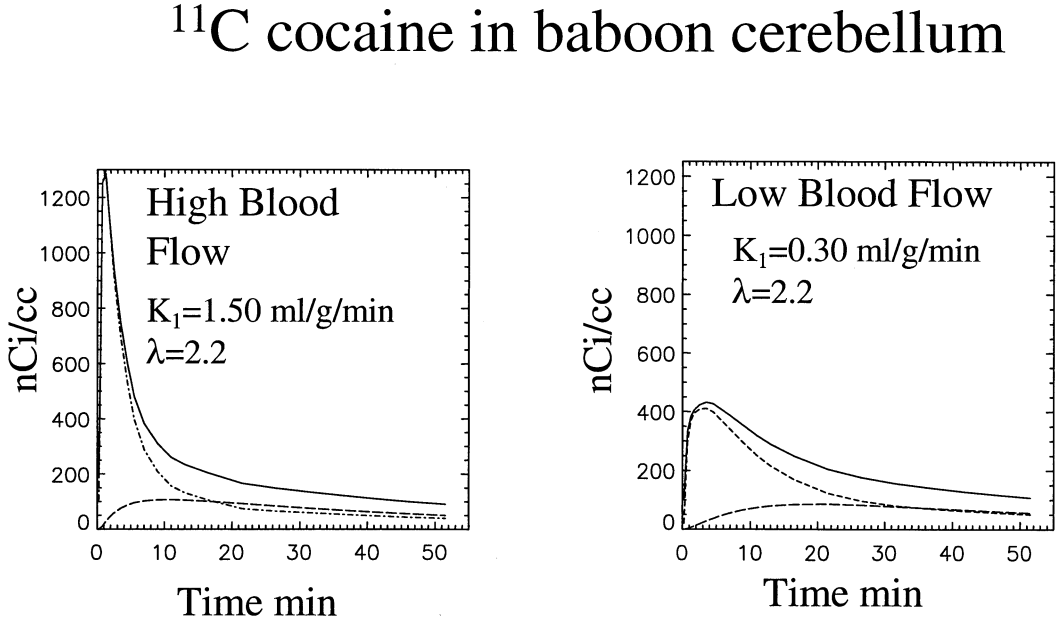

Fig. 8. Simulations of ^{11}C cocaine in the baboon cerebellum under conditions of high and low blood flow. The cerebellum has a slow nonspecific compartment with binding constants and min^{-1} with equilibrium binding constants k_+^{NS}=.025 and k_-^{NS}=k_+^{NS}=.04 min^{-1} with equilibrium binding constant NS=k_+^{NS}/k_-^{NS} = 0.625 and DV = $\lambda(1 + NS)$ = 3.57.

8. Using a reference region input

As with the plasma input function form of the GA equation, the reference region method is also susceptible to noise. Using simulated ROI data without noise both reference region methods give very similar values for the *DVR*, 4.44 and 4.41 for the bilinear and GA respectively (the "true" value is 4.43mL/mL). For comparison the Simplified reference tissue method (SRTM) [27] gives 4.68 for the *DVR*. The SRTM assumes that both receptor and reference region can be adequately described by a 1 tissue compartment model which is not true for this example. Data generated for the simulations above were used to illustrate the noise properties of the *DVR* estimates. For low to moderate noise both methods give similar results, however the bilinear method appears to be less susceptible to noise at the higher levels $DVR = 4.10 \pm 0.21$ and 3.88 ± 0.42 for the GA and bilinear methods respectively. The DVR for the SRTM at this noise level was 5.02.

9. Some problems with reversible tracers

^{11}C cocaine binds reversibly to the dopamine transporter and has been used in a number of studies [28–30]. In recent baboon studies we have encountered poor reproducibility on test/retest which seems to be related to some extent to blood flow. Studies done under different conditions of ventilation resulted in very large differences in blood flow and this appears to affect the value of the *DV*. In order for blood flow to have an effect on the *DV* estimate, implies that the *DV* is being underestimated. A kinetic analysis of the baboon data in a ROI of the cerebellum, which is frequently used as a reference region, reveals a slow nonspecific compartment. This is illustrated in Fig 8 for conditions of low and high blood flow. These simulations are based on actual baboon studies and use a measured plasma input function. The plasma to tissue influx constants were K_1 = 1.5 and 0.3 mL/min/mL (λ = 2.2 mL/mL) for the high and low flow simulations respectively. The slow nonspecific compartment had binding constants $DVR = 6.325/3.57 = 1.77$. The DV is given by $\lambda(1 + NS) = 3.57$ where $NS = k_{+1}^{NS}/k_{-1}^{NS} = 0.625$. The slow nonspecific component represents a small fraction of the total radioactivity at early times <5 min but is equal to the fast nonspecific component at times >20 min. At these later times the total radioactivity is low making the estimate of this slow component difficult. It makes a significant contribution to the total DV. Fig 9 shows the variation in $C_2(t)/(C_1(t) + C_2(t))$ with time. At high blood flow this ratio reaches a constant by 20min while at low blood values it is not quite constant until >30 minutes. This leads to problems in estimating this component under conditions of low blood flow since it is necessary to use data at later times and the half-life of the isotope is short. Introducing a specific binding component with k_3 = 0.6 and $k_4 = 0.48$ min^{-1}, the total DV is given by assuming that *NS* is the same in both the reference region and receptor region. The true *DVR* is given by $DVR = 0.325/3.57 = 1.77$. Results for the analysis of this simulated data under conditions of high and low blood flow varies with the times used for the analysis as shown in Table 3. By terminating the analysis at times less than 40 min the reference region method gives different values for high and low blood flow and these are somewhat different than the values obtained

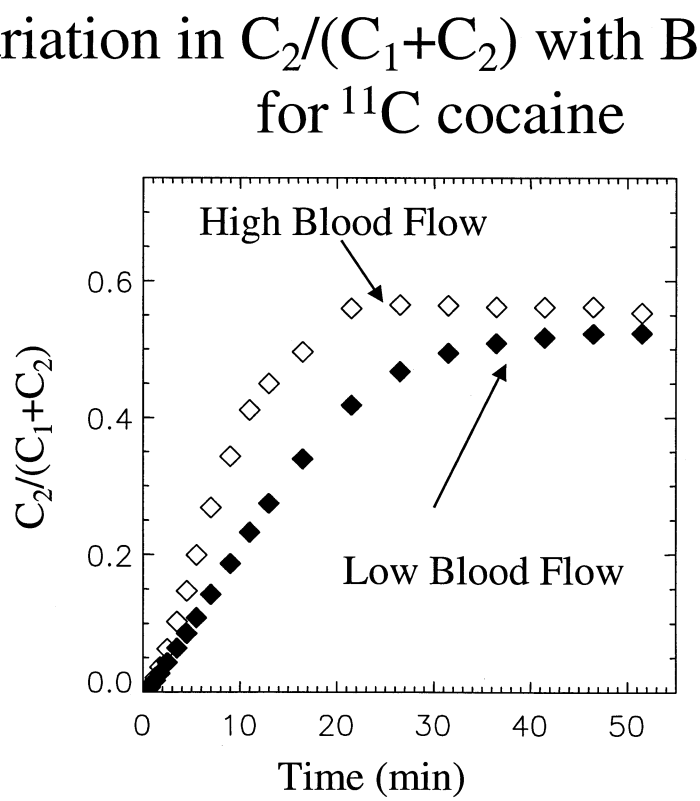

Fig. 9. Variation in $C_2(t)/(C_1(t) + C_2(t)$ with time as a function of blood flow. At high blood flow this ratio reaches a constant by 20min while at low blood values it is not quite constant until $>$ 30 minutes.

using plasma data. While the values for all methods are consistent using longer times, there will also be statistical errors due to the low count rates.

10. Conclusions

The graphical analysis methods originated with the treatment of irreversibly binding tracers. The elegant theoretical work of Patlak [1,9] established the conditions under which the GA method is applicable and was the starting point for the derivation of the method for reversible tracers. The methods are simple to apply and can provide information by a simple plot (Eq. (6a) and Eq. (9) about the type of binding, that is whether it is reversible or irreversible without the necessity of specifying a particular model structure. These techniques are particularly useful in characterizing the kinetics of a new tracer. The simplicity and model independence make graphical methods attractive for the pixel-wise estimation of *DV*, *DVR* or *BP* (derived from the *DVR*). The problem is that the graphical method as formulated in Eq. (6a) underestimates the *DV* in the presence of statistical noise, mostly due to the ROI term in the denominator of the dependent and independent variables [11]. Two methods for dealing with the noise while maintaining the linear method have been proposed. The one with the least bias has been proposed by Ichise [11] and involves rearranging the GA equation into Eq. (10) The bias is greatly reduced by this method but at the expense of increased CV. By using both Eq. (6a) (MLS) and Eq. (10) (GA) and averaging the *DV* estimates from each calculation, an estimate of the *DV* is obtained that has a smaller CV than the MLS method and less bias than the GA. The inclusion of GA in the form of Eq. (6b) may be possible for some tracers, further reducing the bias. By using this combination of analysis methods as well as pixel grouping methods to further reduce noise [26,31] *DV* images may be created with less bias.

Table 3
Variation in DVR calculated with GA under conditions of high and low blood flow

Time* (min)	Reference		Plasma	
	High	Low	High	Low
13–38	1.83	1.68	1.74	1.79
23–43	1.76	1.72	1.72	1.72
23–53	1.72	1.72	1.72	1.72

* Times used for calculating DV or DVR.

Acknowledgments

This work was supported by U.S. D.O.E (OBER; DE-AC02-98CH10886) and N.I.H. (NS-15380).

References

[1] Patlak CS, Blasberg RG, Fenstermacher JD. Graphical evaluation of blood-to-brain transfer constants from multiple-time uptake data. J Cereb Blood Flow Metab 1983;3(1):1–7.

[2] Evans AC. A double integral form of the three compartment, four rate-constant model for faster generation of parametric maps. J Cereb Blood Flow Metab 1987;7(suppl 1):S453.

[3] Blomqvist G. On the construction of functional maps in positron emission tomography. J Cereb Blood Flow Metab 1984;4:629–32.

[4] Logan J, Fowler J, Volkow N, Wolf A, Dewey S, Schlyer D, et al. Graphical analysis of reversible radioligand binding from time-activity measurements applied to [N-11C-methyl]-(-)-cocaine PET studies in human subjects. J Cereb Blood Flow Metab 1990;10(5):740–7.

[5] Logan J, Fowler J, Volkow N, Wang G, Ding Y, Alexoff D. Distribution volume ratios without blood sampling from graphical analysis of PET data. J Cereb Blood Flow Metab 1996;16(5):834–40.

[6] Ichise M, Ballinger JR. From graphical analysis to multilinear regression analysis of reversible radioligand binding. J Cereb Blood Flow Metab 1996;16:750–2.

[7] Ichise M, Fujita M, Seibyl J, Verhoeff N, Baldwin R, Zoghbi S, et al. Graphical analysis and simplified quantification of striatal and extrastriatal dopamine D2 receptor binding with [123I]epidepride SPECT. J Nucl Med 1999;40(11):1902.

[8] Gjedde A. High-, and low-affinity transport of D-glucose from blood to brain. J Neurochem 1981;36(4):1463–71.

[9] Patlak CS, Blasberg RG. Graphical evaluation of blood-to-brain transfer constants from multiple-time uptake data. Generalizations. J Cereb Blood Flow Metab 1985;5(4):584–90.

[10] Slifstein M, Laruelle M. Effects of statistical noise on graphic analysis of PET neuroreceptor studies. Journal of Nuclear Medicine : Official Publication, Soc Nuc Med 2000;41(12):2083–8.

[11] Ichise M, Toyama H, Innis R, Carson R. Strategies to improve neuroreceptor parameter estimation by linear regression analysis. J Cereb Blood Flow Metab 2002;22(10):1271–81.

[12] Logan J, Fowler J, Volkow N, Ding Y, Wang G, Alexoff D. A strategy for removing the bias in the graphical analysis method. J Cereb Blood Flow Metab 2001;21(3):307–20.

[13] Mintun M, Raichle M, Kilbourn M, Wooten G, Welch M. A quantitative model for the in vivo assessment of drug binding sites with positron emission tomography. Ann Neurol 1984;15(3):217–27.

[14] Carson RE, Breier A, de Bartolomeis A, Saunders RC, Su TP, Schmall B, et al. Quantification of amphetamine induced changes in [11C]raclopride binding with continuous infusion. J Cereb Blood Flow Metab 1997;17:437–47.

[15] Lassen NA, Perl W. Tracer Kinetic Methods in Medical Physiology. New York: Raven Press, 1979.

[16] Fowler J, Wang G, Logan J, Xie S, Volkow N, MacGregor R, et al. Selective reduction of radiotracer trapping by deuterium substitution: comparison of carbon-11-L-deprenyl and carbon-11-deprenyl-D2 for MAO B mapping. J Nucl Med 1995;36(7):1255–68.

[17] Fowler J, Volkow N, Logan J, Wang G, MacGregor R, Schyler D, et al. Slow recovery of human brain MAO B after L-deprenyl (Selegeline) withdrawal. Synapse 1994;18(2):86–93.

[18] Fowler JS, MacGregor RR, Wolf AP, Arnett CD, Dewey SL, Schlyer DJ, et al. Mapping human brain monoamine oxide A and B with 11C labeled suicide inactivators and PET. Sci 1987;235:481–5.

[19] Fowler JS, Logan J, Ding Y-S, Franceschi D, Wang G-J, Volkow ND, et al. Non-MAO A binding of clorgyline in white matter in human brain. J Neurochem 2001;79(5):1039.

[20] Logan J, Volkow N, Fowler J, Wang G, Dewey S, MacGregor R, et al. Effects of blood flow on [11C]raclopride binding in the brain: model simulations and kinetic analysis of PET data. J Cereb Blood Flow Metab 1994;14(6):995–1010.

[21] Patlak CS, Fenstermacher JD. Measurements of dog blood-brain transfer constants by ventriculocisternal perfusion. Am J Physiol 1975;229(4):877–84.

[22] Feng D, Wang Z, Huang S-C. A study on statistically reliable and and computationally efficient algorithms for the measurement of cerebral blood flow with positron emission tomography. IEEE Trans Med Imag 1993;12:182–8.

[23] Feng D, Huang S-C, Wang Z, Ho D. An unbiased parametric imaging algorithm for nonuniformly sampled biomedical system parameter estimation. IEEE Transactions on Medical Imaging 1996;15:512–8.

[24] Varga J, Szabo Z. Modified regression model for the Logan plot. J Cereb Blood Flow Metab 2002;22(2):240–4.

[25] Van Huffel S, Vandewalle J. The total least squares problem: computational aspects and analysis. Phildelphia: Society for Industrial and Applied Mathematics, 1991.

[26] Kimura Y, Hsu H, Toyama H, Senda M, Alpert N. Improved signal-to-noise ratio in parametric images by cluster analysis. Neuroimage 1999;9(5):554–61.

[27] Lammertsma AA, Hume SP. Simplified reference tissue model for PET receptor studies. Neuroimage 1996;4(3 Pt 1):153–8.

[28] Volkow N, Fowler J, Logan J, Gatley S, Dewey S, MacGregor R, . Carbon-11-cocaine binding compared at subpharmacological and pharmacological doses: a PET study. J Nucl Med 1995;36(7):1289-2168.

[29] Volkow N, Gatley S, Fowler J, Logan J, Fischman M, Gifford A, et al. Cocaine doses equivalent to those abused by humans occupy most of the dopamine transporters. Synapse 1996;24(4):399–402.

[30] Logan J, Volkow N, Fowler J, Wang G, Fischman M, Foltin R, et al. Concentration and occupancy of dopamine transporters in cocaine abusers with [11C]cocaine and PET. Synapse 1997;27(4):347–56.

[31] Logan J, Fowler J, Ding Y, Franceschi D, Wang G, Volkow N, et al. Strategy for the formation of parametric images under conditions of low injected radioactivity applied to PET studies with the irreversible monoamine oxidase A tracers [11C]clorgyline and deuterium-substituted [11C]clorgyline. J Cereb Blood Flow Metab 2002;22(11):1367–76.